The Journal of Chemical Physics

Noble gas in densified liquid and amorphous silica and thermodynamic conditions for the emergence of bubbles

Cite as: J. Chem. Phys. **155**, 054504 (2021); https://doi.org/10.1063/5.0056362
Submitted: 09 May 2021 • Accepted: 15 July 2021 • Published Online: 03 August 2021

M. Micoulaut and O. Laurent

AIP Publishing

The Journal of Chemical Physics ARTICLE scitation.org/journal/jcp

Noble gas in densified liquid and amorphous silica and thermodynamic conditions for the emergence of bubbles

Cite as: J. Chem. Phys. 155, 054504 (2021); doi: 10.1063/5.0056362
Submitted: 9 May 2021 • Accepted: 15 July 2021 •
Published Online: 3 August 2021

M. Micoulaut[a] and O. Laurent

AFFILIATIONS

Sorbonne Université, Laboratoire de Physique Théorique de la Matière Condensée, CNRS UMR 7600, 4 Place Jussieu, 75252 Paris Cedex 05, France

[a]Author to whom correspondence should be addressed: mmi@lptmc.jussieu.fr

ABSTRACT

Different noble gases (He, Ne, and Ar) containing densified silica liquids and glasses are investigated from molecular dynamics simulations at different system densities using a dedicated force field. The results for pure silica are first compared to reference potentials prior to an investigation of the thermodynamic diagram, the diffusivity, and the structure under different (T, P) conditions. It is found that the equation of state and the diffusivity are weakly sensitive to the nature of the incorporated noble gas, leading to a similar trend with density for all systems. The network structure is weakly altered by the presence of the gas, and pressure induced structural changes are those usually found for amorphous and liquid silica, i.e., Si coordination increase, tetrahedral to octahedral conversion of the base geometry, and collapse of large rings under pressure. Ne- and Ar-based systems display an increased structuration, however, as preferential distances appear in gas–gas correlations at large densities in both the liquid and amorphous states. Finally, we focus on the conditions of heterogeneity that are driven by the formation of noble gas bubbles, and these appear for a threshold density ρ_c that is observed for all systems.

I. INTRODUCTION

The question of the solubility of noble gases in silicate liquids with pressure and with melt composition has not only considerable geophysical implications[1] but also technological ones since inert gases are used in, e.g., glass fiber drawing[2] or heat transfer reduction of window glasses,[3] because the structural properties can be substantially altered.[4] In geochemical studies, while melt composition dependence of noble gas solubility is well-documented at low pressures,[5–10] higher pressure data are more limited,[11–13] but these show that the noble gas solubility increases almost linearly with pressure up to 3 GPa before stabilizing for larger pressures.

For the special case of silica, one expects to have gas solubilities becoming small at elevated pressures because of the compaction of voids inside the structure. However, x-ray and Raman scattering measurements seem to suggest[14,15] that SiO_2 is much less compressible when compressed in helium, as also independently suggested from Brillouin scattering.[16] It is suggested that voids do not fully contract under pressure because of the presence of stuffed helium, albeit obvious structural changes of the host silica matrix are observed. Strong effects on the intermediate-range structural order are obtained, which manifest by a nearly constant behavior of the first sharp diffraction peak position with pressure,[15] at variance with ordinary SiO_2.[17] This means that the incorporation of noble gases is not simply an adsorption phenomenon in a porous media but must involve some modification of the network structure. Similarly, it has been noted that argon solubility drops abruptly for $P \geq 5$ GPa[12] and is weakly dependent on temperature as sets of data with different experimental temperatures[18,19] (1500–3000 K) appear to map onto a single curve, i.e., suggesting negligible temperature dependence of Ar solubility as also observed for more complex silicate melt compositions at high pressures.[20]

Computer simulations appear to be helpful in this context in order to clarify the observed phenomena, and they also provide a detailed atomic scale picture of the effect of noble gas incorporation. A dedicated force field is needed in order to model correctly the silica network and the weakly interacting noble gas, usually modeled by a hard sphere or Lennard-Jones interaction. The limitations of

such potentials are now rather well established. For instance, it has been found that hard sphere models lead to a quasilinear Henry-like behavior increase in the noble gas solubility with pressure,[21,22] in contrast with the current observation. Still, an increased understanding has been obtained. For instance, using molecular dynamics simulations, Guillot and Guissani[23] have evaluated the free energy of the insertion of noble gases in fused silica and have found that the insertion of noble gases into the melt is ruled by the entropy of cavity formation, rather than the solvation energy of the solute atom. This suggests that smaller atoms (e.g., He and Ne) are preferentially solvated with respect to larger ones. Using an *ab initio* potential for liquid silica with argon, Zhang *et al.*[24] established the distribution of interstitial voids in the structure by taking oxygen and silicon atoms as exclusion spheres. The calculated pressure dependence of Ar solubility using this method was found to be in qualitative agreement with the experimental data.[12,19] More recently, Guillot and Sator have established a more accurate force field[25] able to reproduce a certain number of physico-chemical properties of natural silicate melts under various (T, P) conditions.[26,27] These force fields build on three types of components: SiO_2, silica–gas interaction, and gas–gas interaction.[28]

These potentials appear clearly helpful to decode the mechanisms of incorporation of noble gases into silicate melts under pressure. However, a general investigation for all types of noble gases is lacking, and this would permit us to understand the combined effect of pressure, nature of the noble gas, and temperature. The effect of such incorporation of He, Ne, or Ar has often been considered independently for specific systems. The purpose of the present contribution is to perform such systematic studies, i.e., we investigate the structural, thermodynamic, and dynamic properties of He, Ne, and Ar containing liquid silica in the $300 \leq T \leq 4000$ K and $1.2 < \rho \leq 4.2$ g cm^{-3} range by focusing on the effect of the incorporated element. The results indicate that the diffusivity of rare gas containing silica behaves similar to one of the densified liquid silica with (i) anomalies found that manifest by a minimum and a maximum in oxygen diffusivity, (ii) a ring statistics following closely the one determined for SiO_2, and (iii) an equation of state that does not display a very different trend once represented in a $P(\rho)$ diagram. Finally, we determine the density at which noble gas bubbles start to nucleate, and these are found to form below a threshold density ρ_c that depends on the nature of the noble gas particle. On the other hand, the noble gas diffusivity for He and Ne appears to be weakly dependent on T at low density but changing rather dramatically in Ar-bearing liquids.

This paper is organized as follows: Sec. II presents the simulation methods and validates the potential used in this study. Section III presents the results obtained on thermal and structural properties followed by those found for the dynamic properties (Sec. IV). Finally, Sec. V summarizes our findings and draws some conclusions.

II. SIMULATION METHODS

A. System and densification strategies

The simulated liquids and glasses were made of $3000 + N_X$ atoms (X = He, Ne, and Ar) with always a ratio X:Si of 1:10 for the number of species leading to systems of the form SiO_2–$0.1X$ (X = He, Ne, and Ar) and $N_X = 100$. In order to probe the effect of composition, we have also studied SiO_2–0.2He ($N_{He} = 200$). Each system has been first maintained for about 1 ns at 4000 K and 5 GPa in the NPT ensemble. The use of a non-zero pressure is needed in order to avoid the onset of a strongly inhomogeneous liquid driven by noble gas bubble formation (see below). Those liquids were then quenched under this pressure by steps of 500 K down to 300 K with equilibration times of about 300 ps each. Such obtained low temperature systems were used as starting configurations for the other investigated densities by appropriately rescaling the cell length. Densities were changed from 1.3 g cm^{-3} up to 4.2 g cm^{-3}, by increments of 0.1 g cm^{-3}, each new densified system being obtained from its closest counterpart. By using such incremental density steps, the relative variation of bond distances was less than 3%.

Each system has been maintained at a given thermodynamic condition for 100 ps, prior to production runs for 300 ps. It is clear that under certain conditions, certain systems will not fully reach thermodynamic equilibrium, and this turns out to be the case at low temperature (300 K) or at large densities. For the specific Ar-containing silica systems, we have performed longer runs (1 ns) in order to obtain more reliable diffusivity results. Preliminary runs over 300 ps led, indeed, to rather scattered results once represented as a function of system density.

B. Interatomic potential

The gas–gas interactions build on a pair-wise potential of the form

$$V(r) = A_1 e^{-r/\rho_1} - \frac{C_1}{r^6}, \tag{1}$$

where the parameters (A_1, ρ_1, C_1) are fitted in order to reproduce potential energy curves obtained from *ab initio* calculations and the Tang–Toennies van der Waals potentials[29] for rare gas fluids. They are also able to reproduce the equation of state in the (P, V, T) in the thermodynamic diagram for He, Ne, Ar, and Xe at $T = 300$ K, and agreement with experimental data is very good for, e.g., Ar up to 1 GPa.[30]

The interaction potential for silica builds on the Beest–Kramer–Van Santen (BKS) form,[31] and an additional Si–Si interaction is used from the Tsuneyuki–Tsukuda–Aoki–Matsui[32] (TTAM) form. This has been realized previously in order to reproduce the broad Si–O–Si bond angle distribution in amorphous silica and the reduction of its width with the addition of sodium dioxide.[33] An additional highly repulsive term is added at a short distance in order to avoid a spurious collapse of the system at high temperature and elevated pressures.[34]

Finally, we used the fitted parameters of Guillot and Sator[25] to model the noble gas–silica interactions. These authors have acknowledged the lack of theoretical data[35–37] able to realistically reproduce the presence of noble gases in complex magmas and developed, therefore, a potential of the form

$$V_{ij}(r) = 4\varepsilon_{ij}\left[\left(\frac{\sigma_{ij}}{r}\right)^6 - \left(\frac{\sigma_{ij}}{r}\right)^{12}\right], \tag{2}$$

where i is a noble gas of species i (i = He, Ne, and Ar), j is an ion of species j (j = O and Si), r is their separation distance, and ε_{ij} and σ_{ij}

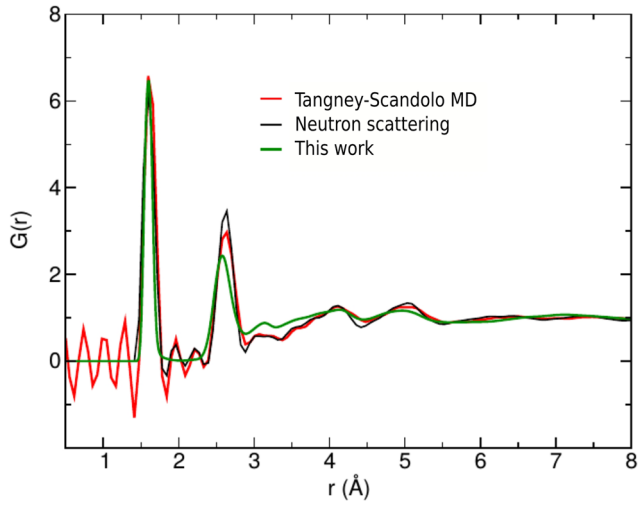

FIG. 1. Calculated pair correlation function $G(r)$ of amorphous SiO_2 at 300 K (green), compared to experimental data from neutron scattering[17] and to results from the Tangney–Scandolo potential.[38]

are the parameters associated with the pair (i,j). These parameters and their physical basis can be found in Ref. 25.

C. Preliminary verification

We have first generated sets of silica liquids under various (ρ, T) conditions and have checked the ability of the potential to properly describe the structure of the base network.

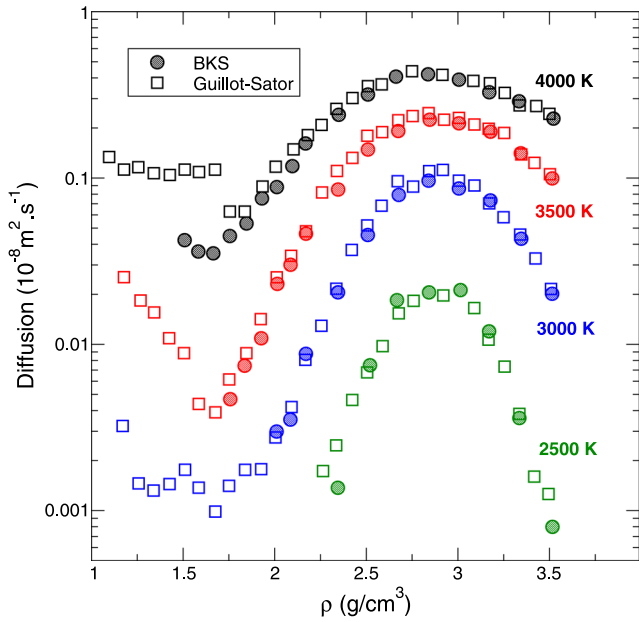

FIG. 2. Calculated oxygen diffusivity D_O in densified silica for different isotherms, compared to previous results.[39]

Figure 1 compares the real-space structure of the obtained silica with experimental data from neutron scattering[17] together with the results obtained from an alternative potential (Tangney–Scandolo[38]). It is seen that characteristic peaks (Si–O distances at 1.65 Å, O–O at 2.70 Å) are well reproduced by the potential. Similarly, we check for the self-diffusion D_α (α = Si, O) for liquid silica, using the definition of the mean-square displacement,

$$\langle r_\alpha^2(t)\rangle = \frac{1}{N_\alpha}\left\langle \sum_{i=1}^{N_\alpha} |\mathbf{r}_{i\alpha}(t) - \mathbf{r}_{i\alpha}(0)|^2 \right\rangle, \tag{3}$$

and the long-time limit of $\langle r_\alpha^2(t)\rangle$ that permits us to obtain the diffusion constant $D_\alpha = \langle r_\alpha^2(t)\rangle/6t$ for all species. Figure 2 represents such diffusivity results as a function of density for various isotherms, and these are found to be compatible with previous results.[39] Specifically, it is found that the usual water-like anomalies[40] observed in tetrahedral liquids are recovered,[41,42] i.e., we find a maximum D_{max} in diffusivity at about 2.9 g cm^{-3}, consistently with previous studies,[39] and a minimum D_{min} at 1.8 g cm^{-3}.

Taken together, both Figs. 1 and 2 provide some confidence that the base system is realistically described and is able to reproduce the salient structural and dynamic features of SiO_2.

III. RESULTS

We now turn to the main results of this contribution, that is, the calculation of thermodynamic, structural, and dynamic properties of densified liquid silica containing noble gases.

A. Equation of state

Figures 3(a) and 3(b) represent the calculated pressure as a function of density for various isotherms for the selection of systems.

For a given system, we first note that the equation of state (EOS) follows a nearly identical trend for densities larger than 2.4 g cm^{-3} at nearly all temperatures (Fig. 3 and inset) but with a progressive deviation to higher pressures at the largest temperature [4000 K, Fig. 3(a)]. This trend is also nearly the same for all systems, although the addition of noble gases leads to an increase in P for $\rho > 2.0$ g cm^{-3}. The pressure is negative for almost all temperatures when $\rho < 2.7$ c cm^{-3}, and this indicates that one has a stretched melt for such conditions [Fig. 3(a)]. Finally, for densities smaller than a certain ρ_1 [e.g., $\rho_1 < 2.3$ g cm^{-3} at 2500 K in silica, Fig. 3(a)], typical Maxwell thermodynamic instabilities onset, resulting in a positive second derivative for the free energy and a negative compressibility ($\chi_T < 0$).

In pure silica [Fig. 3(c)], one, furthermore, finds a probable isobaric density maximum in the region close to ≃3.2 g cm^{-3}, i.e., a minimum in $P(T)$ for selected isochores defining the *locus* of a temperature of maximum density (TMD)[39,40] that is barely notable for the He-containing liquid and evidenced once different isochores are represented [Fig. 3(d)]. In both systems, the temperature at which P is minimum seems to evolve from 2500 K at 3.1 g cm^{-3} to 3500 K at 3.3 g cm^{-3}, albeit not observable for 3.2 g cm^{-3} in the He-containing system. Since this is not the main purpose of this contribution and because our temperature steps are probably too large, it seems difficult to comment more on this. In addition, such TMDs are sometimes found close to the glass transition region (low T, large ρ) so

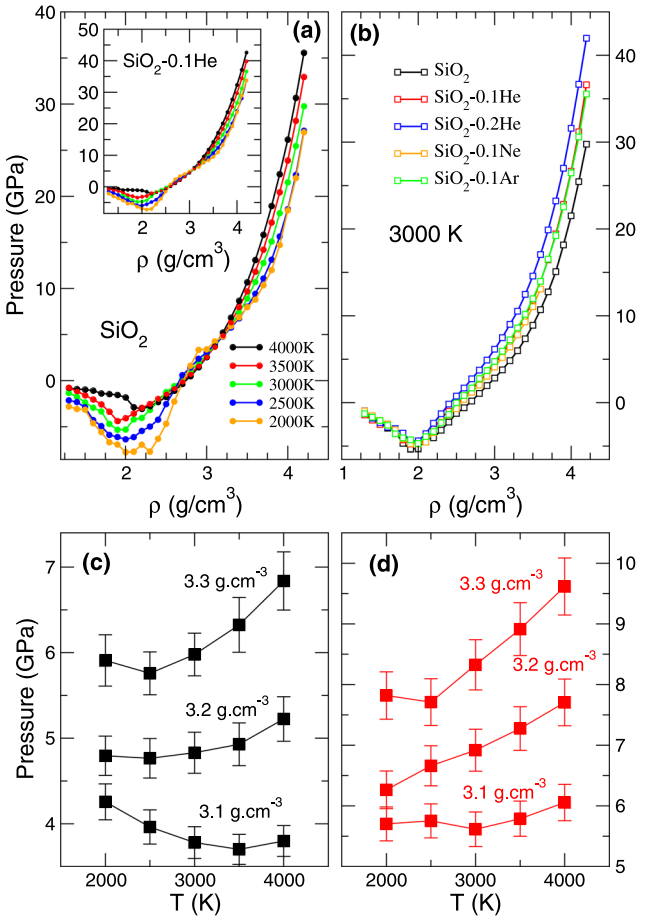

FIG. 3. Calculated equation of state of densified silica containing noble gases. (a) Pure silica at different isotherms ranging from 2000 to 4000 K. The inset shows the equation of state (EOS) of SiO_2–0.1He. (b) EOS of the different systems at 3000 K. (c) $P(T)$ curves in liquid silica for different isochores. (d) $P(T)$ curves in SiO_2–0.1He for different isochores.

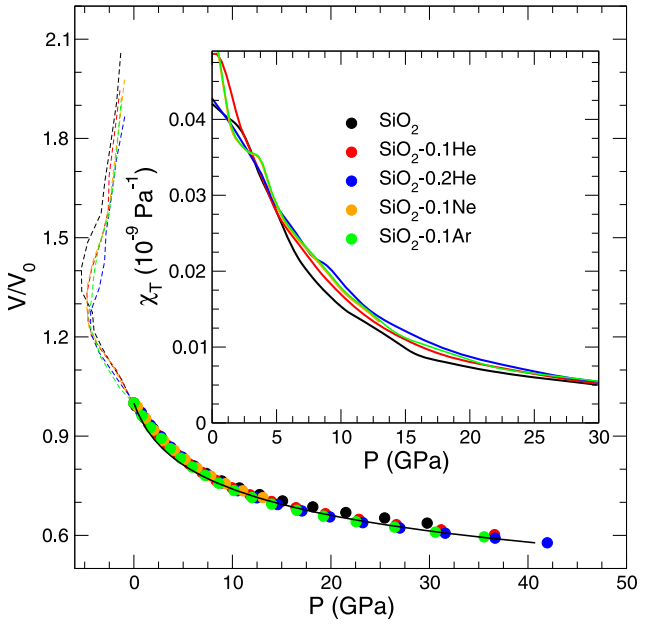

FIG. 4. Equation of state V/V_0 as a function of pressure in liquid silica containing noble gases at 3000 K (symbols). Here, V_0 is the volume at which zero pressure is obtained for each system. Broken lines correspond to the $P < 0$ domain. The solid line represents a Birch–Murnhagan (BH) fit to the $P > 0$ data of the Ne system. The inset shows the isothermal compressibility χ_T as a function of pressure P for the 3000 K isotherm. The colored curves refer to the colored symbols of the main panel.

that the phase space is not fully explored and improved statistics or independent simulations such as Monte Carlo simulations are needed.[39]

It has also to be remarked that for a certain threshold density typically $\rho_c = 2.0$ g cm^{-3}, pressure stops to decrease upon further decompaction and converges to $P \simeq 0$ at low density, this feature being obtained for all noble gas sizes and temperatures (marginally impacted at high temperatures and eventually moving from 2.0 to 2.2 g cm^{-3} for 4000 K). Conversely, for low temperatures (not shown), the same tendencies are obtained, the minimum in $P(\rho)$ becoming more pronounced as also obtained for other typical tetrahedral liquids.[23]

When all systems are being compared, the effect of noble gas concentration appears to dominate with respect to the nature of the noble gas atom [Fig. 3(b)]. For instance, one finds, indeed, 2.83 GPa in silica at $T = 3000$ K, $\rho = 3.0$ g cm^{-3} and for all SiO_2–0.1X systems similar pressures (4.43, 4.10, and 4.74 GPa for X = He, Ne, and Ar, respectively), i.e., somewhat lower than the pressure attained in SiO_2–0.2He (6.15 GPa). In Fig. 4, using these numerical data, we now represent results for the liquid compressibility. We first represent an alternative view of the data of Fig. 3 by plotting the equation of state $V/V_0(P)$ for $P > 0$ (Fig. 4). A Birch–Murnhagan (BH) fit is performed to these data using

$$P = \frac{3}{2}K_0\left[\left(\frac{V}{V_0}\right)^{-7/3} - \left(\frac{V}{V_0}\right)^{-5/3}\right] \times \left[1 + \frac{3}{4}(K_0' - 4)\left(\left(\frac{V}{V_0}\right)^{-2/3} - 1\right)\right], \quad (4)$$

where K_0 is the bulk modulus and K_0' is its derivative. Once applied to the data fulfilling $P > 0$, it leads to a bulk modulus at zero pressure which is of about ≃11–20 GPa (Table I) for nearly all systems in the liquid phase. The functional forms of Eq. (4) then permit one to derive the behavior of the isothermal compressibility $\chi_T = \rho^{-1}(\partial\rho/\partial P)_T$ as a function of system density (inset of Fig. 4), which qualitatively indicates an increased compressibility in silica at elevated pressures and an opposite behavior for $P < 5$ GPa with respect to the liquids containing noble gases.

As expected, the behavior of the EOS in the amorphous phase leads to values for the compressibility that are substantially smaller, e.g., for amorphous silica, it is found that $K_0^{-1} = \chi_T = 0.03(5)$ GPa^{-1}, i.e., somewhat larger than the experimental value determined at zero pressure (0.026 GPa^{-1}[43]). Note that the value of the compressibility depends on the chosen interatomic potential so that χ_T can be found in the range 0.04–0.06 GPa for typical force fields.[44] With

TABLE I. Fitted Birch–Murnhagan (BH) coefficients in 3000 and 300 K silica containing noble gases. Bulk modulus K_0 and first derivative K_0'.

	3000 (K)		300 (K)	
System	K_0 (GPa)	K_0' (GPa)	K_0 (GPa)	K_0' (GPa)
SiO_2	11.5(0)	8.7(9)	28.5(7)	21.2(7)
SiO_2–0.1He	10.8(3)	8.3(7)	27.6(2)	21.0(4)
SiO_2–0.2He	11.5(8)	7.4(0)	29.3(7)	19.3(8)
SiO_2–0.1Ne	18.7(0)	4.2(2)	31.2(4)	15.2(1)
SiO_2–0.1Ar	11.3(0)	7.4(5)	30.3(4)	19.5(1)

the addition of He, the bulk modulus remains at nearly the same level (27.6 GPa for SiO_2–0.1He) and appears to slightly increase with He content, as in the liquid state. These values appear substantially smaller than the ones reported from x-ray diffraction and Raman scattering measurements (K_0 = 110 GPa[14]) but seem compatible with the results from Brillouin scattering (36.5 GPa[16]). Here, two comments have to be made. First, one has to keep in mind that the experiments are performed in a He atmosphere so that the exact atomic concentration of He inside the silica matrix is unknown and can hardly be linked to a fraction investigated in a numerical study (Si:He = 100 and 200). In addition, it has been shown[14] that the nature of the pressure medium was displaying a crucial role as the volume change of silica in a He medium was found to be much smaller than the one in a methanol–ethanol medium. Second, the numbers presented in Table I depend, of course, on the chosen MD model, and previous investigations[44] on the effect of pair potentials on the compressibility of silica have already emphasized the large variability of results. Overall, the present results from the EOS simply indicate (i) an obvious reduction in χ_T with decreasing temperature and (ii) only a moderate increase in K_0 with the addition of noble gases. The investigation of such behaviors with a larger amount of He is currently being considered.

B. Structure

1. Correlations and coordinations

Because of the small fraction of the noble gas inside the structure, we first note that the contribution of corresponding partial structural correlations is very small so that the calculated total pair correlation function $g(r)$ of the different SiO_2–0.1X systems will barely differ from the one represented in Fig. 1. More insightful is the correlation between noble gas atoms. Figure 5 represents such partial correlations g_{XX} (X = He, Ne, and Ar) in amorphous (300 K) and liquid (3000 K) systems.

The correlation between gas atoms displays roughly three typical behaviors as a function of density and temperature. At low density ($\rho < 2.0$ g cm^{-3}), the function g_{XX} indicates the absence of any structural correlations so that no typical interatomic distance can be defined and a homogeneous distribution ($g_{XX} \to 1$) is already found at a short distance (2.5 Å). This feature is typical of a free evolving gas. In this situation, the stretched network with a negative pressure (Fig. 3) leaves sufficient voids to permit an unconstrained motion for the gas particles. These features are also linked with the aspects of inhomogeneities as discussed below. A second regime is acknowledged for intermediate densities at 300 K (roughly from 2.0 to 2.8 g cm^{-3}) that extends to higher densities in the 3000 K liquid ($2.4 \le \rho \le 3.8$ g cm^{-3}). Here, a preferential distance emerges at, e.g., ≃2.8 Å in Ne containing silica but with a homogeneous distribution beyond this first-shell correlation, this feature being observed for all

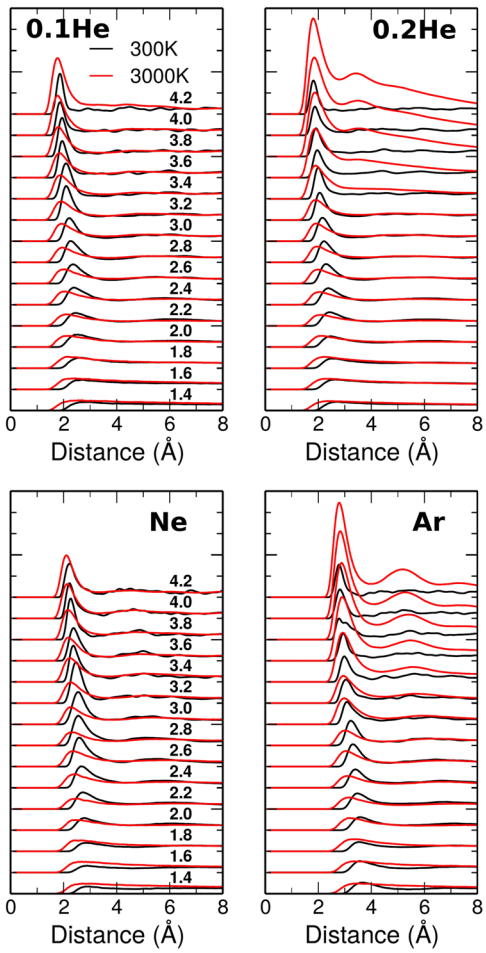

FIG. 5. Calculated pair correlations g_{XX} (X = He, Ne, and Ar) in noble gas containing silica of the form SiO_2–0.1X under ambient (300 K, black) and liquid conditions (3000 K, red) for different system densities ($1.4 \le \rho \le 4.2$ g cm^{-3}).

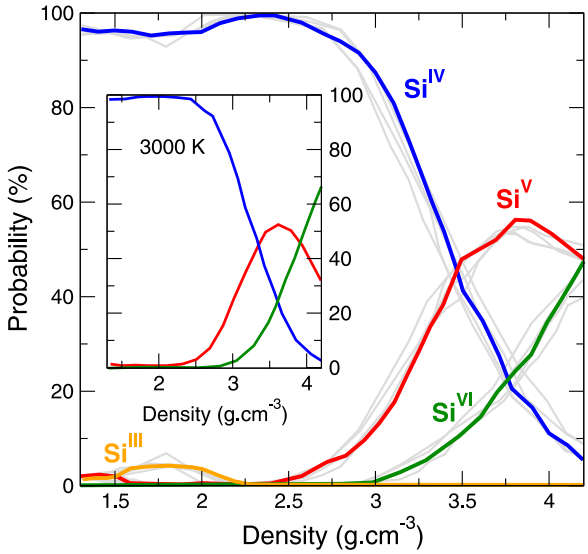

FIG. 6. Calculated Si coordination population in densified amorphous silica (colored curves). The light gray curves correspond to gas (He, Ne, and Ar) containing silica. The inset represents the corresponding calculation for liquid silica at 3000 K.

the investigated systems except for the SiO_2–0.1Ar system, which promotes a secondary preferential distance at ≃5 Å in the liquid. The structure appears to become largely system dependent as He- and Ne-based systems continue to have a nearly homogeneous distribution beyond the first correlating distance, whereas Ar- and the He-rich system (SiO_2–0.2He) now display marked second neighbor correlations, indicative of a structured fluid. This signals obvious size and composition effects.

2. Silicon coordination

The Si coordination number n_{Si} calculated by integrating the pair correlation function $g_{SiO}(r)$ up to its first minimum at r_m = 2.6 Å (not shown) shows very weak dependence on noble gases. As previously found for pure silica,[34] but also for a certain number of silicates,[45,46] the trend exhibits a progressive Si coordination change due to an increased number in oxygen neighbors with growing pressure/density, which also induces the conversion from tetrahedral to Si octahedral local geometries that are typical of the high pressure stishovite polymorph.[47] Specifically, we find that $n_{Si} \simeq 4$ over a wide density range ($1.3 \leq \rho < 2.8$ g cm^{-3}) but with a slight decrease in stretched glasses and liquids ($\rho \leq 1.8$ g cm^{-3}). The evolution of such coordination numbers appears to be weakly influenced by temperature changes (Fig. 6, inset).

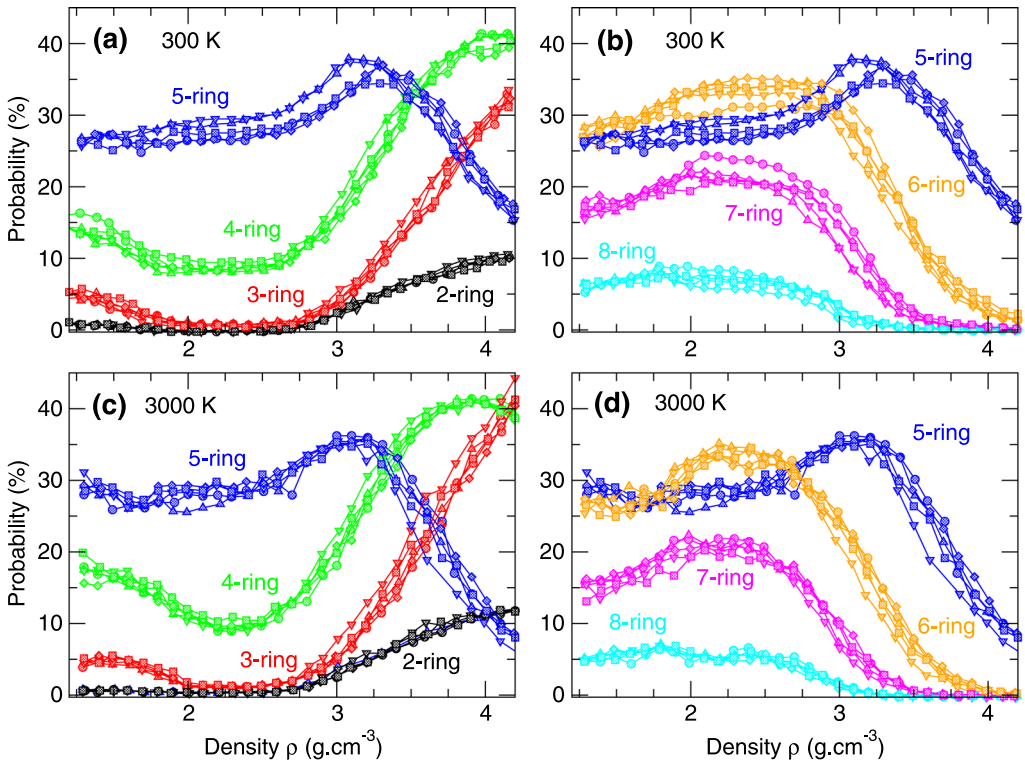

FIG. 7. Calculated ring population at ambient [300 K, panels (a) and (b)] and elevated temperatures [3000 K, (c) and (d)] in densified silica (○), SiO_2–0.1He (△), SiO_2–0.2He (▽), SiO_2–0.1Ne (◇), and SiO_2–0.1Ar (□). (a) and (c) represent the small-ring statistics (n = 2–5), and (b) and (d) represent the larger ring statistics (n = 5–8).

The detail of such coordination numbers (Fig. 6) reveals the usual emergence of fivefold Si (Si^V) with starting densification that grows up to nearly 50% of all Si present and maximizes for ≃3.6 g cm^{-3} as currently observed in densified silica[48,49] and silicates.[50] Upon further densification, a sixfold Si (Si^{VI}) emerges and represents the local coordination of very high pressure. The fraction of Si^{VI} is found to be somewhat lower under ambient conditions (≃50%) as compared to the liquid state (≃70% at 3000 K, inset of Fig. 6). Here, the role of the noble gas atoms in this coordination change with density appears to be negligible as the different Si coordinations are weakly affected by their presence, the fraction of Si^k (k = IV, V, VI) remaining basically the same (gray curves in Fig. 6).

3. Rings

A study of topological intermediate-range order is realized by performing a ring analysis for the different systems and thermodynamic conditions. We use a ring statistics algorithm mostly based on the King–Franzblau[51,52] shortest-path search to find rings containing a maximum of eight silicon atoms. This sort of analysis permits us to have a neat characterization of glassy networks.[53–55]

Figure 7 represents such statistics for silica and noble gas containing silica at ambient [300 K, Figs. 7(a) and 7(b)] and liquid temperatures [3000 K, Figs. 7(c) and 7(d)] as a function of density ρ. For clarity, we have split each ring population and represented small-ring [Figs. 7(a) and 7(c)] and large-ring population [Figs. 7(b) and 7(d)]. Here, it should be noted that by an n-ring, we mean the number of silicon atoms part of the ring. Note that the 5-ring population has been duplicated in order to be used as a reference in all panels.

For pure silica, the general trend with density is in line with previous studies focusing on the effect of pressure on ring population using either experimental or theoretical methods.[17,56–59] Usually, the preliminary stages of compression induce a nearly elastic response and do not alter the ring population.[56] This ambient regime corresponds to the near plateau behavior at intermediate densities [Figs. 7(a) and 7(b)] with 2.0 ≤ ρ ≤ 2.6 g cm^{-3}. Possible plastic events at the nanoscale upon further compression (ρ > 2.6 g cm^{-3}) involve the transformation of tetrahedral silicon into fivefold Q^5 species[45,60] (see also Fig. 6) and a modification of the ring structure, as acknowledged from Fig. 6. Here, the 3- and 4-ring population starts to grow to become the dominant motif of the structure at the expense of 5-rings, and a minority fraction of 2-ring (edge-sharing tetrahedra) typical of chalcogenides[61] is also present at the largest system density (4.2 g cm^{-3}). For the latter, such small 2-, 3-, and 4-rings then represent about 85% of all closed structures, whereas they are only of about ≃20% at 1.2 g cm^{-3}. With increasing pressure (ρ > 3.0 g cm^{-3}), larger rings (5–8) tend to collapse due to volume reduction and to the increased connectivity of the network with the growing population of fivefold and sixfold silicon, which represents the dominant local structure for ρ > 3.5 g cm^{-3} (Fig. 6). This leads, indeed, to an increase in smaller ring structures as also previously acknowledged in chalcogenides[55,61] but also in silica under pressure where the emergence of such smaller rings could be analyzed from a ring zipper mechanism involving a pairing of fivefold and/or sixfold coordinated Si sites.[17] It should finally be noted that the population of fivefold rings has a specific trend with density. In the low densified regime (2.8 < ρ < 3.3 g cm^{-3}) with pressures close to 0 GPa (Fig. 3), fivefold rings appear to be promoted because of two opposite tendencies: (i) the increase in silicon and oxygen coordination numbers, which lead to an increase in the network connectivity and promote small rings, and (ii) the reduction in the molar volume that reduces the possibility to have large rings. Ultimately, the fraction of fivefold rings is about 15% for the highest density.

When the different noble gas containing systems are investigated along the same scheme, it turns out that all behave very similar to pure silica in the liquid state [3000 K, Figs. 7(c) and 7(d)]. For the amorphous systems, we do find that noble gases, in general, tend to increase the fraction of 6-rings to reduce the fraction of sevenfold rings for ρ > 2.0 g cm^{-3}, the fraction of very small rings (2–4) remaining nearly unchanged for all systems over the entire density range.

IV. DIFFUSION AND DYNAMICS

At large temperatures (T > 2500 K), atomic motion is important enough and dynamic properties can be safely computed. Figure 8 now represents the oxygen diffusion coefficient D_O for the different systems as a function of density at different fixed temperatures.

A. Diffusivity anomalies

An inspection of Fig. 8 clearly signals that the well-documented diffusivity anomalies[39] obtained in densified silica (Fig. 2) are maintained with the addition of noble gases. At, e.g., 3000 K, we find for the SiO_2–0.1Ne, indeed, that D_O displays a minimum D_{min} and a maximum D_{max} at 2.0 and 3.4 g cm^{-3}, respectively. The *loci* of D_{min} and D_{max} for the stuffed systems appear to be rather close to those of pure silica, which are usually found at around 2.1–2.3

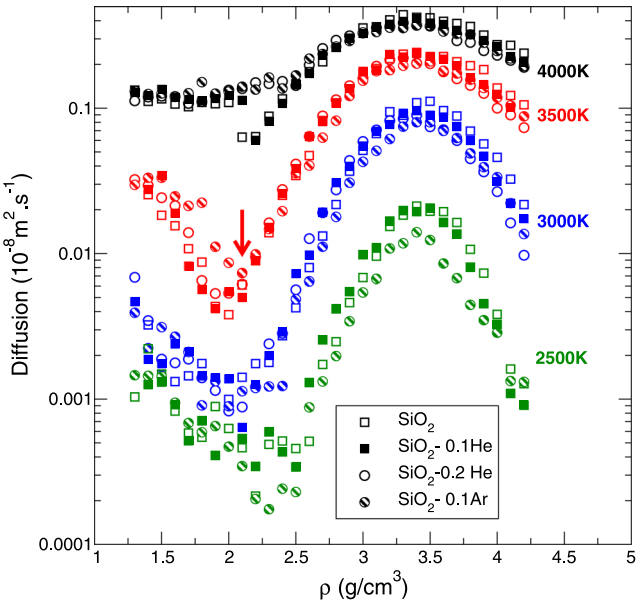

FIG. 8. Calculated oxygen diffusivity D_O in liquid silica and noble gas containing silica as a function of system density for selected isotherms. Note that the silicon diffusivity is about the same as D_O and has not been represented in order to maintain a readable figure. The diffusivities of the SiO_2–0.1Ne have not been represented as they closely follow SiO_2–0.1He.

and 3.2–3.3 g cm^{-3}, respectively, and as for silica, they appear to be coupled with the thermodynamic anomalies noted before (Fig. 3). The minor difference with the reference silica underscores a similar structural change upon densification for the SiO_2–0.1X systems that has been noted before for both the short-range (Fig. 6) and the intermediate-range order (Fig. 7).

When the nature of the noble gas is considered, we note that the presence of argon tends to reduce on the overall the network diffusivity, and at the lowest temperature (2500 K), D_{max} is decreased by nearly a factor of 2 with respect to the helium and neon counterparts. An inspection of Fig. 8 indicates that with decreasing T, differences in network dynamics do emerge and are linked with a progressive distinct structural change for each noble gas, this statement being particularly valid for Ar. For the lightest element, it is, furthermore, seen that the concentration does not play a role at all in the global network dynamics because diffusivities of SiO_2–0.1He and SiO_2–0.2He remain nearly the same. With increasing temperature, these effects tend to vanish, and at the highest considered temperature (4000 K), all investigated systems fall onto the same diffusivity curve.

B. Noble gas diffusivities

Figure 9 now represents the gas diffusivities for the same thermodynamic conditions. Different behaviors are acknowledged between the small and large density regimes and also between the different species stuffing the base silica liquid. For $\rho < 2.3$ g cm^{-3}, diffusion is weakly influenced by temperature conditions, and D_X remains nearly the same as the atomic motion occurs within a stretched silica melt with a large number of voids [Fig. 7(d)]. This feature appears to be generic to all investigated systems [black lines in Figs. 9(a)–9(d)]. As one usually models the diffusivity using a thermally activated process with a functional Arrhenius form $D = D_0 \exp[-E_A/k_BT]$, the present behavior simply signals that the approximate limit of 2.3 g cm^{-3} separates two typical behaviors for the gas particles: a diffusivity process dominated by activation barriers for large system densities and diffusion with $E_A \simeq 0$ at low density.

Once the different systems are being compared, it appears that the concentration does not affect the diffusivity of He-stuffed silica as D_{He} almost behaves very similarly for SiO_2–0.1He and SiO_2–0.2He, and for the lowest considered temperature (2500 K), $D_{He}(\rho)$ is identical. With respect to the latter values, a decrease of about a factor 3 and 20 is obtained for Ne and Ar diffusivities over the entire density interval, respectively.

C. Bubble growth

An additional insight into the dynamics is provided by examining density fluctuations. We separate the simulation box into bins and count the number of atoms inside each bin for a given thermodynamic condition (T, ρ) and average over the entire simulation trajectory. The outcome is a density distribution $f(\rho)$ that

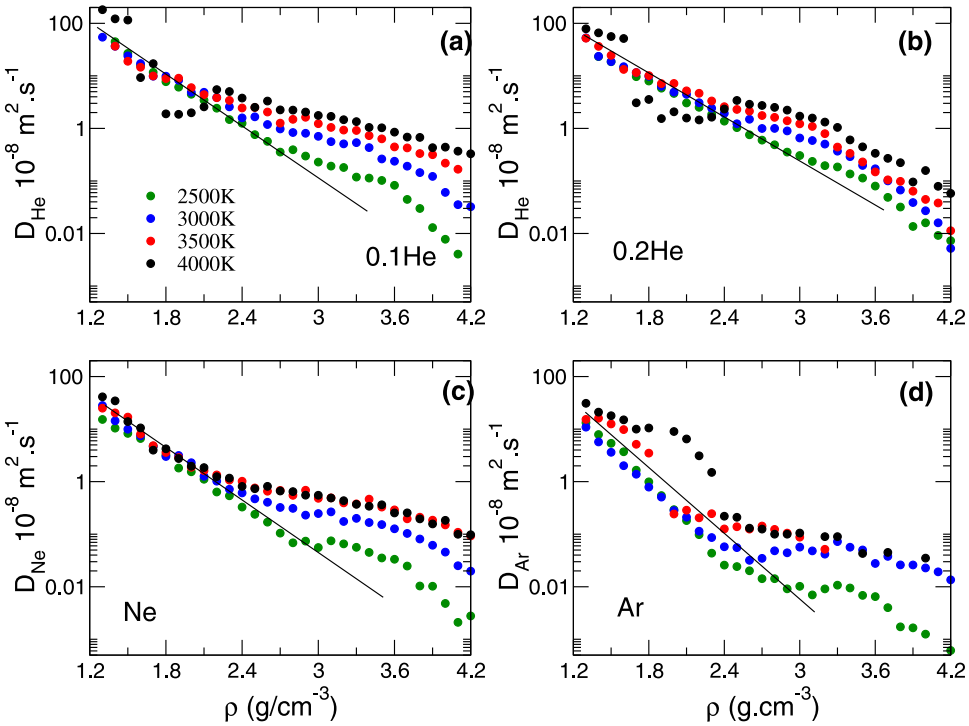

FIG. 9. Calculated gas diffusivities D_X in SiO_2–0.1He (a), SiO_2–0.2He (b), SiO_2–0.1Ne (c), and SiO_2–0.1Ar (d) as a function of system density for selected isotherms. The lines represented in the low density regime serve as a guide.

characterizes the degree of homogeneity of the system and is able to detect the possible occurrence of noble gas bubbles.

To check this method, Fig. 10(a) represents the results for pure silica (3500 K) where the oxygen atom distribution is represented as a function of the nominal (normalized) density ρ_0 for different system densities. As expected, at high density, $f(\rho)$ displays a sharp distribution centered at $\rho = \rho_0$, which is indicative of a homogeneous melt. The situation holds as long as $\rho < 2.2$–2.5 g cm^{-3}, i.e., as long as one has a positive pressure [Fig. 3(a)]. For smaller densities, the distribution obviously broadens, which is indicative of a stretched melt and also the signature of the creation of voids, which induce strong density fluctuations. For our lowest density (1.3 g cm^{-3}), the peak structure of $f(\rho)$ has vanished and one has broad density distribution across the simulation box.

A useful means to characterize these distributions is the calculation of the second moment σ_f of $f(\rho)$, which permits us to follow the broadening of mass distribution inside the simulation box under thermodynamic conditions. Figure 10(b) represents such a second moment as a function of ρ, which permits us to highlight two obvious behaviors. A first one is obtained for densities larger than a threshold density $\rho > \rho_c = 2.0$ g cm^{-3} and exhibits a small value and variation of σ_f, which is the signature of a weak heterogeneity of the structure, albeit the decrease of σ_f between 2.0 and 4.2 g cm^{-3} suggests a continuous refinement of the system homogeneity under pressure. The second regime onsets for $\rho < \rho_c$ and signals that the system has become heterogeneous as σ_f increases and rapidly evolves with decreasing ρ. It is interesting to note that the threshold pressure of $\rho_c = 2.0$ g cm^{-3} coincides with the region of thermodynamic instabilities [Fig. 3(a)] that lead to strong system fluctuations and a diverging isothermal compressibility that promotes bubble formation.

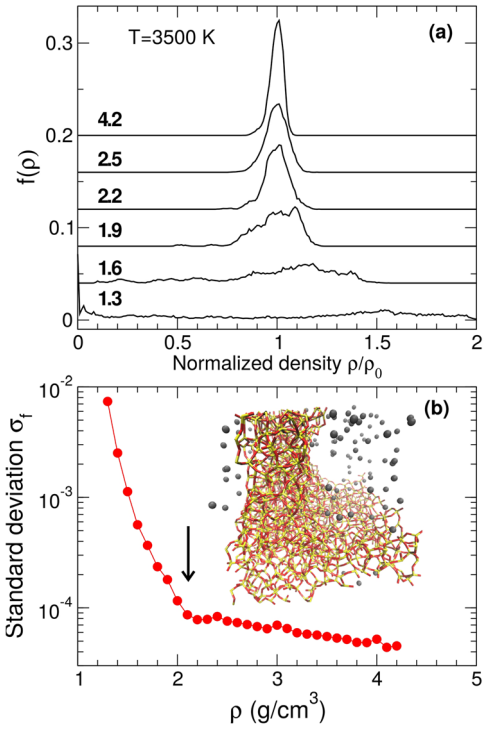

FIG. 10. (a) Mass density distribution $f(\rho)$ across the simulation box as a function of reduced density (ρ/ρ_0) in liquid silica at 3000 K. (b) Evolution of the second moment σ_f of $f(\sigma)$ with system density. The arrow indicates the limit between two obvious low- and high-density regimes. The inset represents a snapshot of the bubble formation in SiO_2–0.1He at 4000 K and 2.1 g cm^{-3}.

1. Low density

We now consider such heterogeneities in the SiO_2–0.1X systems. The regime under consideration corresponds to densities leading to negative pressures for the system (Fig. 3) and to diffusivities of network forming species that are minimum (Fig. 8).

At elevated temperatures, a typical snapshot indicates the formation of noble gas bubbles that will give rise to a certain number of typical behaviors encoded in our previously calculated properties [inset of Fig. 10(b)]. For densities lower than the one displayed (2.1 g cm^{-3}), the system will become increasingly inhomogeneous as manifested by an increase in σ_f (Fig. 11) and by the change in diffusivity (Fig. 9). The formation of these bubbles permits us to understand the salient features displayed in the previously calculated pair correlation functions at low densities. In this regime, as the noble gas atoms are part of a bubble, they behave, indeed, as a free gas and do not exhibit any structuration in pair correlation functions. Here, the first maximum in the pair correlation functions g_{XX} vanish (X = He, Ne, and Ar) and $g_{XX} \to 1$ already at low short distances (≃2 Å, Fig. 5).

2. High density

From Fig. 11, it is, furthermore, noted that noble gas particles induce larger density fluctuations at high density with respect to the reference silica, i.e., for $\rho > 2.4$ g cm^{-3}. The trend is systematic with

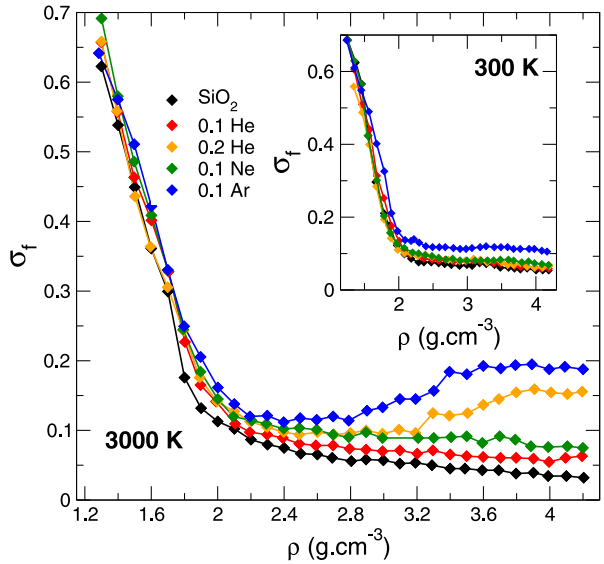

FIG. 11. Evolution of the second moment σ_f of $f(\sigma)$ for different noble gas containing liquid silica at 3000 K. The inset shows the same quantity in the glassy state (300 K).

growing particle size (i.e., from Ne to Ar) and remains for the amorphous system where Ar-based silica appears to display the largest inhomogeneities (inset).

An additional feature emerges in the liquid as a minimal heterogeneity is obtained for the Ar-based and the SiO_2–0.2He liquids between 2.80 and 3.2 g cm^{-3}, and this effect appears to be linked with increased second neighbor correlations between gas particles. All investigated liquids display at large ρ a preferential distance, which manifests by a principal peak in the calculated pair correlation functions g_{XX} at 2–3 Å (Fig. 5). For the two liquids displaying a minima in σ_f, however, the larger density fluctuations occurring at high density (ρ > 3.2 g cm^{-3}) appear to be linked with the presence of a secondary peak at 3.3 and 5.2 Å for SiO_2–0.2He and SiO_2–0.1Ar, respectively (Fig. 5). These anomalies indicate a possible limit in solubility at elevated pressure.

3. Van Hove correlation functions

Additional insight into the real-space dynamics of the stuffed liquids is provided by the Van Hove correlation function,[62,63] which is a density–time correlation of particles. Given that a particle i defines the origin of space coordinates at time $t = 0$, the Van Hove correlation is given as

$$G(\mathbf{r},t) = \frac{1}{N}\left\langle \sum_{i=1}^{N} \delta(\mathbf{r} + \mathbf{r}_i(0) - \mathbf{r}_j(t)) \right\rangle, \tag{5}$$

where $\langle \cdots \rangle$ is the ensemble average over a Dirac delta function $\delta(\cdot)$. The Van Hove correlation function can be divided into a self- and a distinct part for the cases $i = j$ and $i \neq j$, respectively. The former gives indication about an average motion, whereas the latter is directly related to unlike particle correlations that reduce to the static pair correlation function $g(r)$ at $t = 0$.[62] For the self-part, the probability of finding a particle of species α at the position $\mathbf{r}$ at time t is given by

$$4\pi r^2 G_s^{\alpha}(r,t) = \frac{1}{N_{\alpha}}\left\langle \sum_{i=1}^{N_{\alpha}} \delta(\mathbf{r} + \mathbf{r}_i(0) - \mathbf{r}_i(t)) \right\rangle, \tag{6}$$

and $4\pi r^2$ results from the spherical integration of isotropic media. Figure 12 shows the self-part of the van Hove correlation function $G_s^{\alpha}(r,t)$ for the noble gas particles at t = 200 ps for the different liquids at 3000 K. As opposed to the sharper peaks at earlier times which behave as the Dirac $\delta(r)$ for $t = 0$ [Eq. (6)], with the increase in time, the atoms have larger displacements and broader distributions, and eventually extend up to ≃35 Å.

A certain number of comments should be made. First, one acknowledges a global modification of the dynamics of the moving gas particles with increasing density, which evolves from a uniform distribution $G_s(r,t)$ = constant at low density typical of a gas-like behavior[64] to a motion with preferential jump distances (e.g., 20 Å at ρ = 2.5 g cm^{-3} in SiO_2–0.1Ne, Fig. 12) that are clearly influenced by the host silica network structure. Second, as the density is increased, one acknowledges a global reduction in the typical jump distances, which is a salient feature observed before in densified silicates.[65] For instance, for the same Ne-based silica liquid, the dominant jump distance [maximum of $G_s(r,t)$] reduces from 19.4 Å for 2.3 g cm^{-3} to

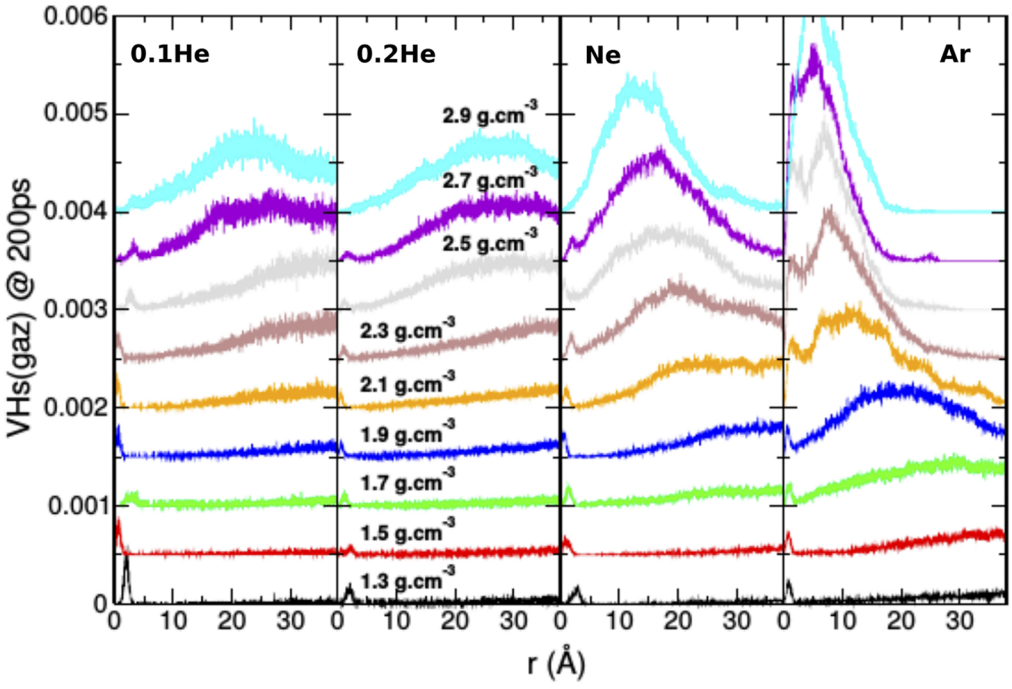

FIG. 12. Self-part of the Van Hove correlation function $G_s(r,t)$ for the different systems as a function of distance, evaluated for t = 200 ps at 3000 K and different system densities. Note that the small peak at a very short distance arises from a single particle contribution.

12.5 Å for 2.9 g cm^{-3}. Third, the typical jump distance decreases with the size of the noble gas particle and appears independent of the concentration given the same $G_s(r,t)$ profile obtained for SiO_2–0.1He and SiO_2–0.2He.

V. SUMMARY AND CONCLUSION

Here, we have performed an extended study of three noble gas containing liquids and glasses using molecular simulations under various (T,ρ) conditions. The results indicate that the equation of state for the liquid and the overall network dynamics (O or Si diffusivity) are weakly sensitive to the addition of noble gases. Conversely, noble gas diffusivities display increased changes as one changes from He to Ne and Ar. The pressure induced structural changes are similar to those obtained for amorphous and liquid silica and lead to a silicon coordination increase and the emergence of octahedral ordering, whereas an increased structuration appears in Ar- and He-rich based silica liquids, which manifests by a more complex profile in Ar–Ar and He–He correlations at elevated densities. The study of the evolution of the intermediate range indicates the collapse of large rings with voids, and this collapse is nearly similar for all investigated systems. Finally, we have focused on the conditions of bubble formation, and these form at densities smaller than a certain threshold density ρ_c, and the results for Ar- and He-rich systems suggest that there are three ways to form such bubbles: (i) either by increasing the size of the noble gas atoms (from He to Ar), consistently with the established reduction in solubility with atom size,[23] (ii) by increasing the noble gas concentration or, finally, (iii) by compressing the liquids in order to reduce interstitial voids that act as hosts at lower pressure and maintain a homogeneous distribution of noble gas atoms in the structure. This latter option becomes particularly obvious as the mass density distribution of the Ar-based system is considered (Fig. 11).

DATA AVAILABILITY

The data that support the findings of this study are available from the corresponding author upon reasonable request.

REFERENCES

[1] A. Paonita, Ann. Geophys. **48**, 647 (2005).
[2] K. Kim, H. S. Kwak, and D. Kim, Comput. Therm. Sci. **4**, 263 (2012).
[3] B. Weller, K. Härth, S. Tasche, and S. Unnewher, *Glass in Building: Principles, Applications, Examples* (Birkhauser, Munich, 2009).
[4] J. Amalberti, P. Burnard, D. Laporte, L. Tissandier, and D. R. Neuville, Geochim. Cosmochim. Acta **172**, 107 (2016).
[5] T. Kirsten, J. Geophys. Res. **73**, 2807, https://doi.org/10.1029/jb073i008p02807 (1968).
[6] A. Hayatsu and C. E. Waboso, Chem. Geol. **52**, 97 (1985).
[7] A. Jambon, H. Weber, and O. Braun, Geochim. Cosmochim. Acta **50**, 401 (1986).
[8] H. Walter, K. Roselieb, H. Büttner, and M. Rosenhauer, Am. Mineral. **85**, 1117 (2000).
[9] M. G. Mesko and J. E. Shelby, Phys. Chem. Glasses **43**, 283 (2002).
[10] G. Iacono-Marziano, A. Paonita, A. Rizzo, B. Scaillet, and F. Gaillard, Chem. Geol. **279**, 145 (2010).
[11] B. C. Schmidt and H. Keppler, Earth Planet. Sci. Lett. **195**, 277 (2002).
[12] M. A. Bouhifd, A. P. Jephcoat, and S. P. Kelley, Chem. Geol. **256**, 252 (2008).
[13] M. A. Bouhifd and A. P. Jephcoat, Nature **439**, 961 (2006).
[14] T. Sato, N. Funamori, and T. Yagi, Nat. Commun. **2**, 345 (2011).
[15] G. Shen, Q. Mei, V. B. Prakapenka, P. Lazor, S. Sinogeikin, Y. Meng, and C. Park, Proc. Natl. Acad. Sci. U. S. A. **108**, 6004 (2011).
[16] C. Weigel, A. Polian, M. Kint, B. Rufflé, M. Foret, and R. Vacher, Phys. Rev. Lett. **109**, 245504 (2012).
[17] A. Zeidler, K. Wezka, R. F. Rowlands, D. A. J. Whittaker, P. S. Salmon, A. Polidori, J. W. E. Drewitt, S. Klotz, H. E. Fischer, M. C. Wilding, C. L. Bull, M. G. Tucker, and M. Wilson, Phys. Rev. Lett. **113**, 135501 (2014).
[18] M. R. Carroll and E. M. Stolper, Geochim. Cosmochim. Acta **57**, 5039 (1993).
[19] E. Chamorro-Perez, P. Gillet, and A. Jambon, Earth Planet. Sci. Lett. **145**, 97 (1996).
[20] A. Montana, Q. Guo, S. L. Boettcher, B. S. White, and M. Brearley, Am. Mineral. **78**, 1135 (1993).
[21] P. Sarda and B. Guillot, Nature **436**, 95 (2005).
[22] B. Guillot and P. Sarda, Geochim. Cosmochim. Acta **70**, 1215 (2006).
[23] B. Guillot and Y. Guissani, J. Chem. Phys. **105**, 255 (1996).
[24] C. Zhang, Z. Duan, and M. Li, Geochim. Cosmochim. Acta **74**, 4140 (2010).
[25] B. Guillot and N. Sator, Geochim. Cosmochim. Acta **80**, 51 (2012).
[26] G. J. Aubry, N. Sator, and B. Guillot, Chem. Geol. **343**, 85 (2013).
[27] T. Dufils, N. Sator, and B. Guillot, Chem. Geol. **493**, 298 (2018).
[28] Y. Liang, C. R. Miranda, and S. Scandolo, High Pressure Res. **28**, 35 (2008).
[29] K. T. Tang and J. P. Toennies, J. Chem. Phys. **118**, 4976 (2003).
[30] C. Tegeler and R. Span, and W. Wagner, J. Phys. Chem. Ref. Data **28**, 779 (1999).
[31] B. W. H. van Beest, G. J. Kramer, and R. A. van Santen, Phys. Rev. Lett. **64**, 1955 (1990).
[32] S. Tsuneyuki, M. Tsukada, H. Aoki, and Y. Matsui, Phys. Rev. Lett. **61**, 869 (1988).
[33] M. Bauchy, Ph.D. thesis, Université Pierre et Marie Curie, France, 2012.
[34] M. Micoulaut, Chem. Geol. **213**, 197 (2004).
[35] R. J.-M. Pellenq and D. Nicholson, J. Phys. Chem. **98**, 13339 (1994).
[36] M. D. Macedonia, D. D. Moore, E. J. Maginn, and M. M. Olken, Langmuir **16**, 3823 (2000).
[37] Z. Du, N. L. Allan, J. D. Blundy, J. A. Purton, and R. A. Brooker, Geochim. Cosmochim. Acta **72**, 554 (2008).
[38] P. Tangney and S. Scandolo, J. Chem. Phys. **117**, 8898 (2002).
[39] M. S. Shell, P. G. Debenedetti, and A. Z. Panagiotopoulos, Phys. Rev. E **66**, 011202 (2002).
[40] J. R. Errington and P. G. Debenedetti, Nature **409**, 318 (2001).
[41] M. Agarwal, M. Singh, B. Shadrack Jabes, and C. Chakravarty, J. Chem. Phys. **134**, 014502 (2011).
[42] F. Pacaud and M. Micoulaut, J. Chem. Phys. **143**, 064502 (2015).
[43] O. B. Tsiok, V. V. Brazhkin, A. G. Lyapin, and L. G. Khvostantsev, Phys. Rev. Lett. **80**, 999 (1998).
[44] A. M. Walker, L. A. Sullivan, K. Trachenko, R. P. Bruin, T. O. H. White, M. T. Dove, R. P. Tyer, I. T. Todorov, and S. A. Wells, J. Phys.: Condens. Matter **19**, 275210 (2007).
[45] M. Bauchy and M. Micoulaut, Nat. Commun. **6**, 6398 (2015).
[46] M. E. Fleet and G. S. Henderson, Phys. Chem. Miner. **24**, 345 (1997).
[47] T. Sato and N. Funamori, Phys. Rev. Lett. **101**, 255502 (2008).
[48] F. Yuan and L. Huang, Sci. Rep. **4**, 5035 (2015).
[49] Y. Zhang, L. Huang, and Y. Shi, Nano Lett. **19**, 5222 (2019).
[50] M. Bauchy, B. Guillot, M. Micoulaut, and N. Sator, Chem. Geol. **346**, 47 (2013).
[51] S. V. King, Nature **213**, 1112 (1967).
[52] D. S. Franzblau, Phys. Rev. B **44**, 4925 (1991).
[53] X. Yuan and A. N. Cormack, Comput. Mater. Sci. **24**, 343 (2002).
[54] M. Micoulaut, X. Yuan, and L. W. Hobbs, J. Non-Cryst. Solids **353**, 1951 (2007).
[55] M. Bauchy, A. Kachmar, and M. Micoulaut, J. Chem. Phys. **141**, 194506 (2014).
[56] L. P. Dávila, M.-J. Caturla, A. Kubota, B. Sadigh, T. Díaz de la Rubia, J. F. Shackelford, S. H. Risbud, and S. H. Garofalini, Phys. Rev. Lett. **91**, 205501 (2003).
[57] M. Okuno, B. Reynard, Y. Shimada, Y. Syono, and C. Willaime, Phys. Chem. Miner. **26**, 304 (1999).
[58] Y. Liang, C. R. Miranda, and S. Scandolo, Phys. Rev. B **75**, 024205 (2007).

[59]P. McMillan, B. Piriou, and R. Couty, J. Chem. Phys. **81**, 4234 (1984).
[60]B. Mantisi, A. Tanguy, G. Kermouche, and E. Barthel, Eur. Phys. J. B **85**, 304 (2012).
[61]M. Micoulaut, A. Kachmar, M. Bauchy, S. Le Roux, C. Massobrio, and M. Boero, Phys. Rev. B **88**, 054203 (2013).
[62]L. Van Hove, Phys. Rev. **95**, 249 (1954).
[63]W. Kob and H. C. Andersen, Phys. Rev. E **51**, 4626 (1995).
[64]J. P. Hansen and R. Mac Donald, *Theory of Simple Liquids* (Elsevier, Amsterdam, 2013).
[65]M. Bauchy and M. Micoulaut, Phys. Rev. B **83**, 184118 (2011).